

Scaling and High-Frequency Performance of AlN/GaN HEMTs

Xi Luo¹, Subrata Halder¹, Walter R. Curtice¹, James C. M. Hwang¹, Kelson D. Chabak², Dennis E. Walker, Jr.², and Amir M. Dabiran³

¹Lehigh University, Bethlehem, PA 18015, USA

²Air Force Research Laboratory, Wright Patterson AFB, OH 45433, USA

³SVT Associates, Inc., Eden Prairie, MN 55344, USA

Email: xil609@lehigh.edu

Abstract — Small- and large-signal RF characteristics were measured on AlN/GaN HEMTs with 80-160 nm gate length and 100-300 μm width. Consistent with the literature, current-gain cut-off frequency and maximum frequency of oscillation were found to increase with inverse gate length and independent of gate width. For the first time, output power and efficiency were reported at the high end of X-band, and were comparable to the best reported at 2 GHz and insensitive to gate length or width. These results suggest that the AlN/GaN HEMTs can be further scaled for even higher frequency and higher power performance.

Index Terms — Cutoff frequency, gallium compounds, HEMTs, microwave transistors, pulse measurement, power measurement.

I. INTRODUCTION

Of all high-electron-mobility transistors (HEMTs), the AlN/GaN HEMT has the highest carrier density and adequate mobility, which result in the highest channel conductance [1]. With AlN as thin as a few nanometers, the AlN/GaN HEMT has also the highest mutual transconductance and can be aggressively scaled for millimeter-wave power applications without short-channel effects [2]. With record-setting DC characteristics of AlN/GaN HEMTs, about two-dozen papers have been published [3]-[26] since 2006 on small-signal characteristics such as the current-gain cut-off frequency f_T and the maximum frequency of oscillation f_{MAX} (Table I). Fig. 1 shows the scaling of f_T and f_{MAX} with the gate length L_G . In general, f_T increases with inverse L_G with $f_T \cdot L_G \approx 10 \pm 6 \text{ GHz} \cdot \mu\text{m}$. However, scaling of L_G was systematically investigated only in [3] and [7], and the gate width W_G was always fixed. Large-signal characteristics were reported in [9], [10], [13], [17] only at an operating frequency $f = 2 \text{ GHz}$, with saturated output power $P_{SAT} = 0.5\text{-}2.6 \text{ W}$ per mm gate width at a drain-source voltage $V_{DS} \approx 15 \text{ V}$. This paper further explores scaling of both L_G and W_G , especially concerning their effects on small- and large-signal RF characteristics at X-band.

II. EXPERIMENTAL

The present AlN/GaN heterostructure was grown on a c-plane sapphire substrate by plasma-assisted molecular beam epitaxy with a 0.7- μm -thick AlGaIn buffer layer, a

TABLE I
RF CHARACTERISTICS OF ALN/GAN HEMTs

L_G (μm)	W_G (μm)	f_T^a (GHz)	f_{MAX}^a (GHz)	f (GHz)	P_{SAT} (W/mm)	PAE (%)	Reference
0.06- 0.25	50 \times 2	83- 31	139- 89				[3]
0.1	50 \times 2	87	149				[4]
0.2	10	52	60				[5], [8]
0.25	15	24	52				[6]
0.05- 0.2	50 \times 2	106- 49					[7]
1	200	6	11	2	0.85	24	[9], [10]
1	200	10	32				[11], [16]
0.25		60					[12]
2		3.5					
1.3	150	9	32	2	2.6	33	[13]
0.4	200	20	31				[14]
0.15	150 \times 2	25	22				[15]
0.15		50	102	2	0.53	41	[17]
3	100	3	8				[18]
0.4	200	20	37				[19]
0.08	38 \times 2	112	215				[20]
0.2	100	80	65				[21], [26]
0.5		40	55				
0.15	25 \times 2	75	115				[22]
0.15	38 \times 2	82	210				[23]
		50	150				
0.2	100	50	40				[24]
0.16	50	85	103				[25]
0.08		68	103		2.7	31	
0.12	50 \times 2	57	82		2.4	32	
0.16		50	76		2.2	29	
0.08		72	114		2.6	30	
0.12	100 \times 2	63	96	12	2.3	33	This Work
0.16		51	77		2.1	31	
0.08		72	97		2.3	26	
0.12	150 \times 2	55	90		2.1	27	
0.16		50	80		2.0	24	

^aExtrinsic values from as-measured S-parameters whenever possible.

2- μm -thick GaN channel layer, a 3.5-nm-thick AlN barrier layer, and a 1-nm-thick GaN cap layer. The combination of GaN and its native oxide helped passivate the surface and suppress gate leakage. (100-nm-thick SiN passivation was added beside the gate.) The gate metal NiAu was patterned by electron-beam lithography into gates of $L_G = 80 \text{ nm}$, 120 nm , and 160 nm . Each gate was centrally located in a 2.7- μm spacing between source and drain Ti/Al/Ni/Au metals. Each HEMT contained two gate fingers with $W_G = 50 \times 2 \mu\text{m}$, $100 \times 2 \mu\text{m}$, or $150 \times 2 \mu\text{m}$. Details of material growth and device processing can be found in [1] and [15], respectively.

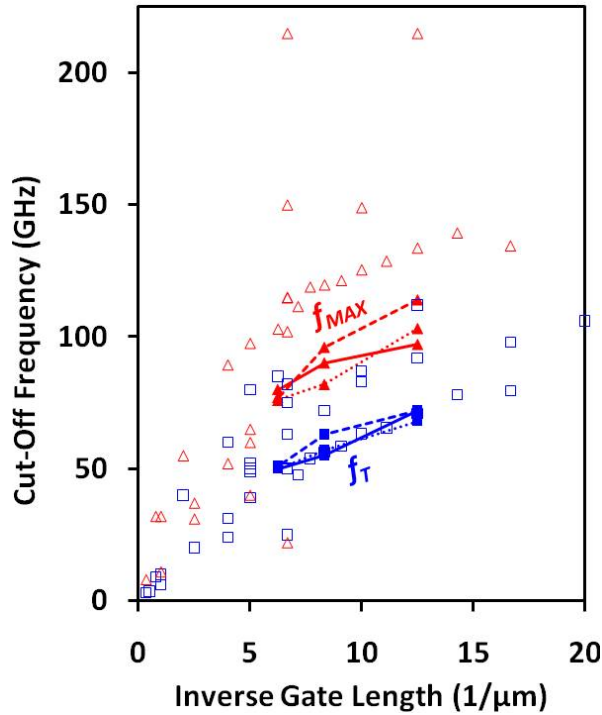


Fig. 1. Published (\square) f_T and (\triangle) f_{MAX} of AlN/GaN HEMTs vs. measured (\blacksquare) f_T and (\blacktriangle) f_{MAX} in this work. $W_G = (\cdot \cdot \cdot)$ $50 \times 2 \mu\text{m}$, $(- - -)$ $100 \times 2 \mu\text{m}$, or $(—)$ $150 \times 2 \mu\text{m}$.

The HEMTs were characterized on-wafer. Small-signal characteristics were measured from 6 to 40 GHz in a 50- Ω system. The resulted S -parameters were used to extract f_T , f_{MAX} , and other equivalent-circuit parameters [27]. Large-signal characteristics were measured at $f = 12$ GHz under optimum input and output matches. To minimize heating, both V_{DS} and the RF input power P_{IN} were turned on for only 1 μs with a repetition frequency of 2.78 KHz. RF output power P_{OUT} was sampled in the middle of the pulse.

III. DC AND SMALL-SIGNAL CHARACTERISTICS

Van der Pauw measurement showed that the present AlN/GaN HEMTs had a carrier density of $\sim 3 \times 10^{13} \text{ cm}^{-2}$ and a carrier mobility of $\sim 800 \text{ cm}^2/\text{V}\cdot\text{s}$, which resulted in a sheet resistivity of $\sim 300 \Omega/\square$. Transmission-line measurement confirmed that the sheet resistivity was $279 \pm 31 \Omega/\square$. Typically, the HEMTs exhibited a pinch-off voltage of approximately -2 V with a subthreshold slope of ~ 0.5 V/decade, a saturated drain current of ~ 500 mA/mm at $V_{GS} = 0$, and an extrinsic transconductance $G_M \approx 500$ mS/mm. The off-state drain-source breakdown voltage was approximately 20 V; the off-state drain-gate breakdown voltage was approximately 40 V. The gate leakage current was $< 100 \mu\text{A}/\text{mm}$. The contact resistance was $\sim 0.5 \Omega\cdot\text{mm}$; the total source resistance was $\sim 1 \Omega\cdot\text{mm}$;

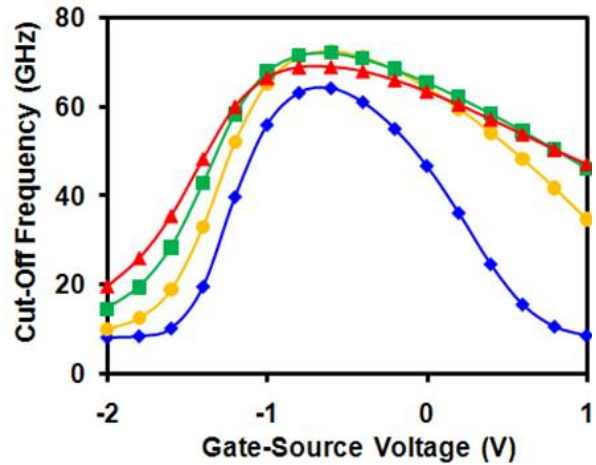


Fig. 2. Measured f_T of present AlN/GaN HEMT. $L_G = 80$ nm. $W_G = 100 \times 2 \mu\text{m}$. $V_{DS} = (\blacklozenge)$ 2 V, (\blacksquare) 4 V, (\bullet) 6 V, or (\blacktriangle) 8 V.

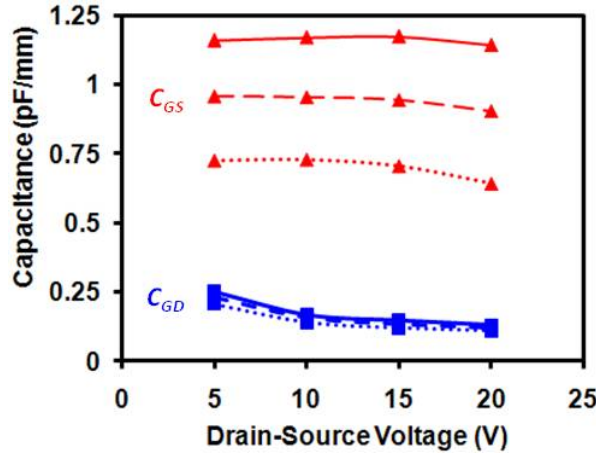


Fig. 3. Measured (\blacktriangle) C_{GS} and (\blacksquare) C_{GD} of present AlN/GaN HEMTs. $L_G = (\cdot \cdot \cdot)$ 80 nm, $(- - -)$ 120 nm, or $(—)$ 160 nm. $W_G = 150 \times 2 \mu\text{m}$. $V_{GS} = -0.2$ V.

the total channel and drain resistance was $\sim 2 \Omega\cdot\text{mm}$; the gate resistance was $\sim 5 \Omega\cdot\text{mm}$. Detailed discussions of the DC characteristics can be found in [28].

Fig. 1 shows also that f_T and f_{MAX} of the present HEMTs increase with inverse gate length and follow closely the trend established by the pioneering work of [3], except f_{MAX} is approximately 20% lower probably due to higher output conductance caused by higher buffer leakage [28]. There is no significant dependence on gate width, which suggests that up to $150 \mu\text{m}$ per finger width is tolerable up 40 GHz. Fig. 2 shows that typical of all present HEMTs, f_T peaks around $V_{GS} = -0.6$ V and is fairly constant for $V_{DS} > 2$ V – the knee voltage V_{KNEE} . Fig. 3 shows that, although the gate capacitance decreases with decreasing gate length, there is a fixed parasitic component on the order of 0.1 pF/mm. This will eventually cause gate length scaling to

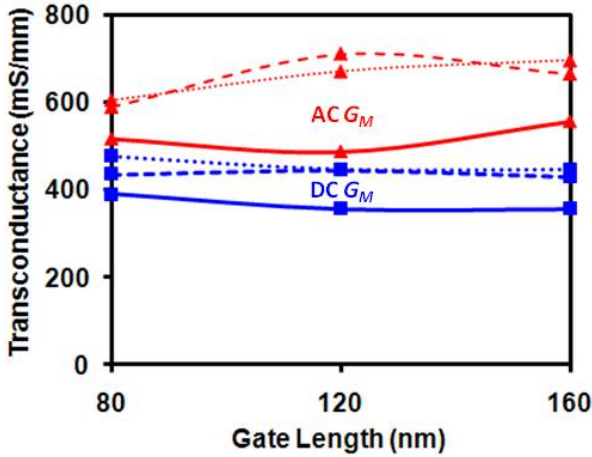


Fig. 4. Measured (■) DC G_M vs. extracted (▲) AC G_M of present AlN/GaN HEMTs. $W_G = (\cdot\cdot\cdot) 50 \times 2 \mu\text{m}$, $(- - -) 100 \times 2 \mu\text{m}$, or $(—) 150 \times 2 \mu\text{m}$.

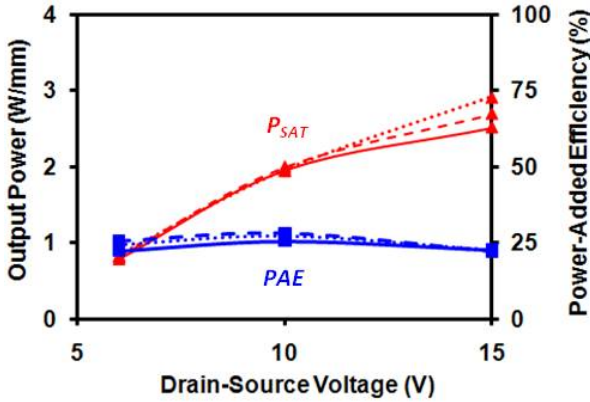


Fig. 5. Measured (▲) P_{SAT} and (■) PAE of present AlN/GaN HEMTs. $L_G = (\cdot\cdot\cdot) 80 \text{ nm}$, $(- - -) 120 \text{ nm}$, or $(—) 160 \text{ nm}$. $W_G = 150 \times 2 \mu\text{m}$. $V_{GS} = -1 \text{ V}$. $V_{DS} = 7 \text{ V}$. $f = 12 \text{ GHz}$.

reach diminishing return. As expected, the gate-source capacitance C_{GS} is relatively independent of V_{DS} , while the gate-drain capacitance C_{GD} decreases rapidly with increasing V_{DS} . Fig. 4 shows that the extracted AC transconductance is actually higher than the measured DC transconductance, which indicates that the present HEMTs are not as dispersive as earlier ones.

IV. LARGE-SIGNAL CHARACTERISTICS

As listed in Table I, although both saturated output power density P_{SAT} and power-added efficiency PAE of the present HEMTs decrease with increasing gate length and width, the dependence is not very strong. This suggests that there is ample room to scale the HEMTs for higher power. Although both P_{SAT} and PAE were measured at a much higher frequency than that of [13],

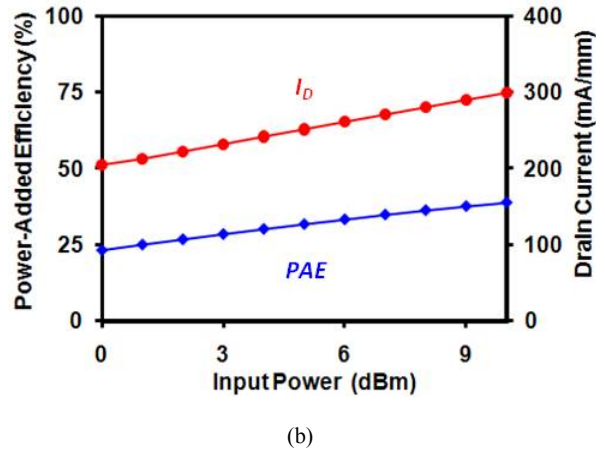
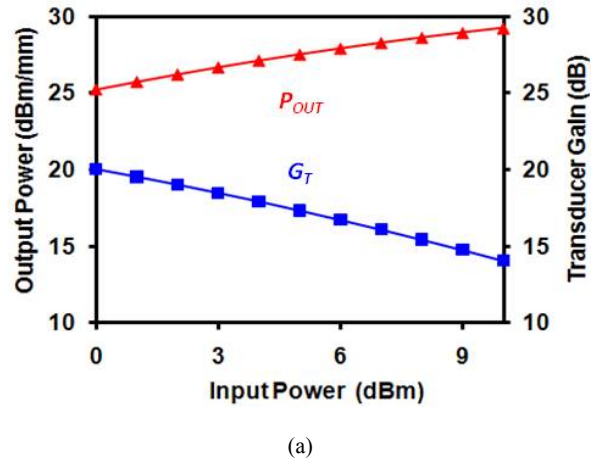


Fig. 6. Measured (a) (▲) P_{OUT} and (■) transducer gain G_T , and (b) (●) drain current I_D , and (◆) PAE and for present AlN/GaN HEMT. $L_G = 160 \text{ nm}$. $W_G = 150 \times 2 \mu\text{m}$. $V_{GS} = -1 \text{ V}$. $V_{DS} = 7 \text{ V}$. $f = 12 \text{ GHz}$.

their values were comparable. In both cases, $P_{SAT} \approx 2.5 \text{ W/mm}$ is quite reasonable for $V_{DS} \approx 15 \text{ V}$, $V_{KNEE} \approx 2 \text{ V}$, and $I_{MAX} \approx 1 \text{ A/mm}$, where I_{MAX} is the maximum open-channel current. Fig. 5 shows that P_{SAT} increases with V_{DS} sub-linearly and increasing V_{DS} beyond 15 V would degrade the HEMTs by generating and trapping hot electrons under the gate [29]. By contrast, PAE is independent of V_{DS} and is in general low for these relatively small devices. Fig. 6 shows that low PAE is probably caused by soft gain compression due to buffer leakage.

V. CONCLUSION

For the gate lengths and widths investigated in this work, the AlN/GaN HEMTs appear to scale well and consistent with the literature. This suggests that there is room for further scaling to achieve even higher frequency

and higher power performance. Although the present output power density appears to be reasonable, it can be improved by evening out the field distribution between the gate and the drain to minimize the generation of hot electrons, and by improving the quality of the gate stack to avoid trapping any hot electron generated. Similarly, although short-channel effects appear to be under control, they can be further suppressed by reducing buffer leakage.

ACKNOWLEDGEMENT

This work was supported in part by the US National Aeronautics and Space Administration under contract no. NNX09C76C.

REFERENCES

- [1] A. M. Dabiran, A. M. Wowchak, A. Osinsky, J. Xie, B. Hertog, B. Cui, D. C. Look, and P. P. Chow, "Very high channel conductivity in low-defect AlN/GaN high electron mobility transistor structures," *Applied Physics Lett.*, vol. 93, no. 8, p. 082111, Aug. 2008.
- [2] G. Jessen, R. Fitch, J. Gillespie, G. Via, A. Crespo, D. Langley, D. Denninghoff, M. Trejo, and E. Heller, "Short-channel-effect limitations on high-frequency operation of AlGaIn/GaN HEMTs for T-gate devices," *IEEE Trans. Electron Devices*, vol. 54, no. 10, pp. 2589-2597, Sep. 2007.
- [3] M. Higashiwaki, T. Mimura, and T. Matsui, "AlN/GaN insulated-gate HFETs using Cat-CVD SiN," *IEEE Electron Device Lett.*, vol. 27, no. 9, pp. 719-721, Sep. 2006.
- [4] M. Higashiwaki, T. Mimura, and T. Matsui, "Enhancement-mode AlN/GaN HFETs using Cat-CVD SiN," *IEEE Trans. Electron Devices*, vol. 54, no. 6, pp. 1566-1570, June 2007.
- [5] Y. Cao, T. Zimmermann, D. Deen, J. Simon, J. Bean, N. Su, J. Zhang, P. Fay, H. Xing, and D. Jena, "Ultrathin MBE-grown AlN/GaN HEMTs with record high current densities," in *Dig. Int. Semiconductor Device Research Symp.*, Dec. 2007.
- [6] D. Deen, T. Zimmermann, Y. Cao, D. Jena, and H. G. Xing, "2.3 nm barrier AlN/GaN HEMTs with insulated gates," *Physica Status Solidi C*, vol. 5, no. 6, pp. 2047-2049, May 2008.
- [7] N. Onojima, N. Hirose, T. Mimura, and T. Matsui, "Ultrathin AlN/GaN heterostructure field-effect transistors with deposition of Si atoms on AlN barrier surface," *Applied Physics Lett.*, vol. 93, p. 223501, June 2008.
- [8] T. Zimmermann, D. Deen, Y. Cao, J. Simon, P. Fay, D. Jena, and H. G. Xing, "AlN/GaN insulated-gate HEMTs with 2.3 A/mm output current and 480 mS/mm transconductance," *IEEE Electron Device Lett.*, vol. 29, no. 7, pp. 661-664, July 2008.
- [9] S. Seo, G. Y. Zhao, and D. Pavlidis, "Power characteristics of AlN/GaN MISFETs on sapphire substrate," *Electronics Lett.*, vol. 44, no. 3, pp. 244-245, July 2008.
- [10] S. Seo, K. Ghose, G. Y. Zhao, and D. Pavlidis, "AlN/GaN metal insulator semiconductor field effect transistor on sapphire substrate," *IEICE Trans. Electronics*, vol. E91-C, no. 7, pp. 994-1000, July 2008.
- [11] S. Seo, E. Cho, and D. Pavlidis, "Improvements of AlN/GaN MISFET DC and RF characteristics with *in situ* deposited Si₃N₄," *Electronics Lett.*, vol. 44, no. 24, pp. 244-245, Nov. 2008.
- [12] T. Zimmermann, Y. Cao, D. Jena, H. G. Xing, and P. Saunier, "4-nm AlN barrier all binary HFET with SiN_x gate dielectric," *Int. J. High Speed Electronics Systems*, vol. 19, no. 1, pp. 153-159, Mar. 2009.
- [13] D. A. Deen, S. C. Binari, D. F. Storm, D. S. Katzer, J. A. Roussos, J. C. Hackley, and T. Gougousi, "AlN/GaN insulated gate HEMTs with HfO₂ gate dielectric," *Electronics Lett.*, vol. 45, no. 8, pp. 423-424, Apr. 2009.
- [14] C. Y. Chang, T. J. Anderson, F. Ren, S. J. Pearton, A. M. Dabiran, A. M. Wowchak, B. Cui, and P. P. Chow, "Very low sheet resistance AlN/GaN high electron mobility transistors," in *Compound Semiconductor Manufacturing Technology Conf. Dig.*, May 2009.
- [15] K. Chabak, A. Crespo, D. Tomich, D. Langley, V. Miller, M. Trejo, J. K. Gillespie, G. D. Via, A. M. Dabiran, A. M. Wochak, B. Cui, and P. P. Chow, "Processing methods for low ohmic contact resistance in AlN/GaN MOSHEMTs," in *Compound Semiconductor Manufacturing Technology Conf. Dig.*, May 2009.
- [16] E. Cho, S. Seo, C. Jin, D. Pavlidis, G. Fu, J. Tuerck, and W. Jaegermann, "Impact of *in situ* SiN, layer grown with metal organic vapor phase epitaxy on the electrical and optical properties of AlN/GaN metal insulator semiconductor field effect transistor structures," *J. Vacuum Science Technology B*, vol. 27, no. 5, pp. 2079-2083, Sep./Oct. 2009.
- [17] S. Seo, E. Cho, G. Aroshvili, C. Jin, D. Pavlidis, and L. Considine, "Dispersion, high-frequency and power characteristics of AlN/GaN metal insulator semiconductor field effect transistors with *in-situ* MOCVD deposited Si₃N₄," *IEICE Trans. Electronics*, vol. E93-C, no. 8, pp. 1245-1249, Aug. 2010.
- [18] S. Taking, A. Z. Khokhar, D. MacFarlane, S. Sharabi, A. M. Dabiran, and E. Wasige, "New process for low sheet and ohmic contact resistance of AlN/GaN MOS-HEMTs," in *Proc. European Microwave Integrated Circuits Conf.*, Sep. 2010, pp. 306-309.
- [19] C. Y. Chang, C. F. Lo, F. Ren, S. J. Pearton, I. I. Kravchenko, A. M. Dabiran, B. Cui, and P. P. Chow, "Normally-on/off AlN/GaN high electron mobility transistors," *Physica Status Solidi C*, vol. 7, no. 10, pp. 2415-2418, Oct. 2010.
- [20] A. L. Corrion, K. Shinohara, D. Regan, I. Milosavljevic, P. Hashimoto, P. J. Willadsen, A. Schmitz, D. C. Wheeler, C. M. Butler, D. Brown, S. D. Burnham, and M. Micovic, "Enhancement-mode AlN/GaN/AlGaIn DHFET with 700-mS/mm g_m and 112-GHz f_T ," *IEEE Electron Device Lett.*, vol. 31, no. 10, pp. 1116-1118, Oct. 2010.
- [21] S. Taking, D. MacFarlane, A. Z. Khokhar, A. M. Dabiran, and E. Wasige, "DC and RF performance of AlN/GaN MOS-HEMTs," in *Proc. Asia-Pacific Microwave Conf.*, Dec. 2010, pp. 445-448.
- [22] D. A. Deen, D. F. Storm, R. Bass, D. J. Meyer, D. S. Katzer, S. C. Binari, J. W. Lacin, and T. Gougousi, "Atomic layer deposited Ta₂O₅ gate insulation for enhancing breakdown voltage of AlN/GaN high electron mobility transistors," *Applied Physics Lett.*, vol. 98, no. 2, p. 023506, Jan. 2011.
- [23] D. F. Brown, K. Shinohara, A. Williams, I. Milosavljevic, R. Grabar, P. Hashimoto, P. J. Willadsen, A. Schmitz, A. L. Corrion, S. Kim, D. Regan, C. M. Butler, S. D. Burnham, and M. Micovic, "Monolithic integration of enhancement- and depletion-mode AlN/GaN/AlGaIn DHFETs by selective MBE regrowth," *IEEE Trans. Electron Devices*, vol. 58, no. 4, pp. 1063-1067, Apr. 2011.
- [24] S. Taking, D. MacFarlane, and E. Wasige, "AlN/GaN MOS-HEMTs with thermally grown Al₂O₃ passivation," *IEEE Trans. Electron Devices*, vol. 58, no. 5, pp. 1418-1424, May 2011.
- [25] F. Medjdoub, M. Zegaoui, N. Waldhoff, B. Grimbert, N. Rolland, and P.-A. Rolland, "Above 600mS/mm transconductance with 2.3A/mm drain current density AlN/GaN high-electron-mobility transistors grown on silicon," *Applied Physics Express*, vol. 4, no. 6, p. 064106, June 2011.
- [26] S. Taking, D. MacFarlane, and E. Wasige, "AlN/GaN-based MOS-HEMT technology: processing and device results," *J. Active Passive Electronic Components*, vol. 2011, p. 821305, 2011.
- [27] J. Deng, W. Wang, S. Halder, W. R. Curtice, J. C. M. Hwang, V. Adivarahan, and A. Khan, "Temperature-dependent RF large-signal

model of GaN-based MOSHFETs,” *IEEE Trans. Microwave Theory Techniques*, vol. 56, pp. 2709-2716, Dec. 2008.

- [28] K. D. Chabak, D. E. Walker Jr., A. Crespo, M. Trejo, M. Kossler, S. Tetlak, J. K. Gillespie, G. D. Via, A. Dabiran, A. M. Wowchak, and P. P. Chow, “Small signal and DC characteristics of ultra-thin GaN/AlN/GaN HFETs,” *Int. J. High Speed Electronics Systems*, accepted for publication.
- [29] R. Vetry, N. Q. Zhang, S. Keller, and U. K. Mishra, “The impact of surface states on the DC and RF characteristics of AlGaIn/GaN HFETs,” *IEEE Trans. Electron Devices*, vol. 48, no. 3, pp. 560-566, Mar. 2001.